Photoluminescence Enhancement and Structure Repairing of Monolayer $MoSe_2$ by Hydrohalic Acid Treatment

Hau-Vei Han,[¶ #, †] Ang-Yu Lu,[#,†] Li-Syuan Lu,[§] Jing-Kai Huang,[#] Henan Li,[#] Chang-Lung Hsu,[‡] Yung-Chang Lin,[&] Ming-Hui Chiu,[#] Kazu Suenaga,[&] Chih-Wei Chu,[‡] Hao-Chung Kuo,[¶*] Wen-Hao Chang,[§,||] Lain-Jong Li[#,*] and Yumeng Shi[#,*]

[#]*Physical Sciences and Engineering Division, King Abdullah University of Science and Technology, Thuwal, 23955-6900*

[¶]*Department of Photonics and Institute of Electro-Optical Engineering, National Chiao Tung University, Hsinchu, Taiwan*

[§]*Department of Electrophysics, National Chiao Tung University, Hsinchu, Taiwan.*

[||] *Taiwan Consortium of Emergent Crystalline Materials (TCECM), Ministry of Science and Technology, Taiwan.*

[‡]*Research Center for Applied Sciences, 128 Sec. 2, Academia Rd., Nankang, Taipei 11529, Taiwan*

[&]*National Institute of Advanced Industrial Science and Technology (AIST), Tsukuba, Japan*

[*]To whom correspondence should be addressed: (H.C. Kuo) hckuo@faculty.nctu.edu.tw; (L. J. Li) lance.li@kaust.edu.sa; (Y. Shi) yumeng.shi@kaust.edu.sa

† These authors contribute equally

KEYWORDS: Transition metal dichalcogenides; Molybdenum diselenide; Layered materials; Photoluminescence; Two-dimensional materials.

BRIEFS: The photoluminescence of defective $MoSe_2$ can be significantly enhanced by HBr doping.

ABSTRACT

Atomically thin two-dimensional transition metal dichalcogenides (TMDCs) have attracted much attention recently due to their unique electronic and optical properties for future optoelectronic devices. Chemical vapor deposition (CVD) method is able to generate TMDCs layers with a scalable size and a controllable thickness. However, the TMDC monolayers grown by CVD may incorporate structural defects and it is fundamentally important to understand the relation between photoluminescence and structural defects. In this report, point defects (Se vacancies) and oxidized Se defects in CVD-grown $MoSe_2$ monolayer are identified by transmission electron microscopy and X-ray photoelectron spectroscopy. These defects can significantly trap free charge carriers and localize excitons, leading to the smearing of free band-to-band exciton emission. Here we report that the simple hydrohalic acid treatment (such as HBr) is able to efficiently suppress the trap state emission and promote the neutral exciton and trion emission in defective $MoSe_2$ monolayers through the *p*-doping process, where the overall photoluminescence intensity at room temperature can be enhanced by a factor of 30. We show that HBr treatment is able to active distinctive trion and free exciton emissions even from highly defective $MoSe_2$ layers. Our results suggest that the HBr treatment not only reduces the *n*-doping in $MoSe_2$ but also reduces the structural defects. The results provide further insights of the control and tailoring the exciton emission from CVD-grown monolayer TMDCs.

Table of Content

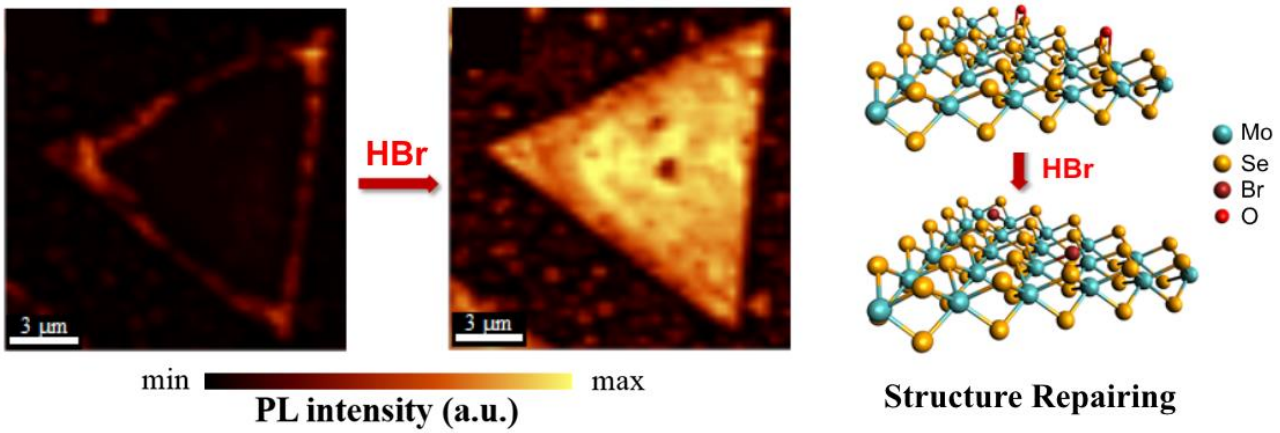

Atomically thin transition metal dichalcogenides (TMDCs) can be obtained by mechanical [1, 2] or chemical exfoliation [3] from their bulk crystals. Due to their unique and striking properties, monolayer TMDCs have attracted extensive attention. Semiconducting TMDC monolayers have been demonstrated feasible for various energy related applications, where their electronic properties [1, 4, 5] and high surface areas offer opportunities for applications such as biosensors, [6, 7] nano generators, [8] green electronics, [9] electrocatalytic hydrogen generation [10, 11] and energy storage. [12, 13] Semiconducting TMDC monolayers, such as MoS_2, [14-16] WS_2, [17-19] $MoSe_2$ [20, 21] and WSe_2, [22-25] exhibit direct band gaps and show attractive light emission properties in the visible and near-infrared spectral region, making them suitable for optoelectronic devices. [26] Applications based on TMDCs in light emitting diodes, [27] and photodetectors [28, 29] have been developed recently. Significant efforts have been devoted to the control and tuning of photoluminescence (PL) properties in TMDCs. Several approaches including electrostatic gating, [30] chemical treatment, [31-33] surface plasmonic excitation, [34] photonic crystal cavities [35] and strain engineering [36, 37] have been adopted to modulate the trions and neutral excitons in monolayer TMDCs. CVD-grown TMDC layers could exhibit unique PL property which is absent in their exfoliated TMDC counterparts. For example, extraordinary PL has been observed near the edge of CVD grown WS_2 recently. [17] Edges and point defects in monolayer TMDCs formed during CVD could be engineered to tailor their electronic, optical and catalytic properties. [38-42] Interestingly, the structural defects in TMDCs have been reported to darken and blue shift the PL peak in MoS_2 and WS_2 [38]. Controversially, recent reports have also demonstrated that point defects could activate PL in TMDCs and increase the overall PL intensity. [39] It still demands more experimental efforts to understand the point defects and excitonic characteristics in TMDC layers.

Chemical doping is known as an effective way to modulate the optical and electrical properties of TMDCs. Matsuda *et al*. have reported that the PL intensity of mechanically exfoliated MoS_2 monolayer can be enhanced when it is interacted with a *p*-dopant 2,3,5,6-tetrafluoro-7,7,8,8-tetracyanoquinodimethane (F4TCNQ), where the *p*-doing can switch the recombination of negative trions to the neutral exciton.[32] Yet, the PL intensity enhancement ratio is only around 3 with the F4TCNQ

doping.[32] More recently, Amani *et al*. have reported that PL and minority carrier lifetime in exfoliated MoS_2 monolayers can be uniformly enhanced by an organic super acid treatment. [43] However, the exact mechanism by which the passivation of surface defects is not fully understood. Furthermore, in the previous studies, the modulation of PL properties in TMDCs by surface chemistry and structural defect engineering have been mostly limited to mechanically exfoliated TMDCs. [31, 32, 38, 39] Compared to the exfoliation method, CVD-grown TMDCs are more practical for large scale device applications. [44] Since the CVD-grown TMDCs may exhibit a wide range of defect types and defect density levels, different from the mechanically exfoliated TMDCs, the defect and optical emission relations are yet to be explored.

In this contribution we demonstrate that the PL intensity of monolayer $MoSe_2$ grown from CVD can be effectively enhanced after exposure to hydrohalic acid vapors, such as HCl, HBr and HI. The overall PL intensity of $MoSe_2$ dramatically increases for more than 30 times by HBr treatment. Due to the structural defects that commonly exist in CVD grown TMDCs, neutral exciton and trion peaks are rarely observed in low temperature PL measurement. We found the defect trapped exciton can be greatly suppressed by the HBr treatment which allow us to observe the neutral exciton and trion peaks from CVD grown $MoSe_2$. Furthermore, our scanning transmission electron microscope (STEM) characterization proves the presence of point defects in $MoSe_2$ structures. Raman spectrum, PL, X-ray photoelectron spectroscope (XPS) and STEM suggest that the HBr treatment imposes various effects which explain the PL enhancement such as removing impurities, *p*-doping to the $MoSe_2$, and reducing the structure of $MoSe_2$.

RESULTS AND DISCUSSIONS

Monolayer $MoSe_2$ was grown via the CVD process according to our previous reports, [21] where sulfur and MoO_2 powders were used as precursors. Figure 1a illustrates the optical micrograph (OM) of the CVD $MoSe_2$ monolayers synthesized on sapphire substrates, where the monolayer $MoSe_2$ exhibits a triangular shape with the lateral size up to 10 μm. Here, we use hydrohalic acids as highly efficient agents to tune the exciton PL in $MoSe_2$ monolayers grown by CVD. Figure 1b schematically illustrates the experimental set-up for the hydrohalic acid treatment. Aqueous solutions of HCl, HBr and HI were bubbled and brought

to the sample by Ar gas, and the $AgNO_3$ was used to absorb the exhaust gas. Photoluminescence from the as-grown and treated $MoSe_2$ monolayers excited by a 532 nm laser are shown in Figure S1. Only one high intensity peak with photon energy around 1.53 eV was observed in both pristine and HBr treated $MoSe_2$, which is close to the reported band gap of 1.55 eV for monolayer $MoSe_2$. Figure 1c compares the PL intensity spatial mappings for as-grown and treated $MoSe_2$. As shown in Figure 1d and 1e, PL signals are pronounced at the edge of the as-grown $MoSe_2$ and become very weak or absent towards the centre of the as-grown monolayer $MoSe_2$. A blue-shift was also observed from the centre to the edge. Recently, a similar phenomenon has been observed on CVD-grown WS_2 monolayer by Yu and *et al*, [40] where they suggest that the defects within the crystal act as non-radiative recombination sites and thus quench the intrinsic PL. Consistently, the edge enhanced PL emission has been observed in CVD grown WS_2 monolayer in previous studies, and the darkening of PL in the centre of TMDCs island has be attributed to the charge defect-induced doping.[17, 45] Our result shows that the overall PL intensity of $MoSe_2$ dramatically increases for more than 30 times after HBr treatment, which suggests the PL tunability of defective monolayer $MoSe_2$. Figures 1d and 1e display the PL line scans for PL intensity and photon energy across the sample before and after HBr treatment, respectively. Remarkably, the PL intensity increases significantly and the photon energy blue shifts at the centre of the triangle. For the spatial modulation of PL intensities and positions in $MoSe_2$, various factors are responsible, including external electrostatic doping, structural defect and chemical composition change. The darkening of PL in the centre of $MoSe_2$ islands is attributable to the presence of structural defects such as point defects and dislocations within the metastable nuclei. [38] During the CVD growth procedure, the initial nucleation occurs at the beginning of the growth process followed by the incoming $MoSe_2$ species coalescing into the nuclei leading to an enlarged $MoSe_2$ grain. Therefore, the HBr molecules are more likely to adsorb at the nucleation centre of $MoSe_2$ and results in a more pronounced PL change. In addition to HBr, other hydrohalic acids such as HCl, and HI also show similar PL enhancement effects (see Figure S2). Among the three hydrohalic acids, HBr shows the best PL enhancement performance. In a previous report, [46] the light emission in mechanically exfoliated TMDC flakes were shown to be sensitive to H_2O molecules.

We have separately examined the effect of moisture and no significant PL enhancement is observed with only H_2O treatment (details in supporting Figure S3). Therefore, the effect of moisture can be excluded in this study. Furthermore, we have also excluded other possible gaseous adsorption effects, such as O_2, by comparing the PL intensity change in vacuum for the sample before and after HBr treatment (details in supporting Figure S4). All the results consistently indicate HBr plays a major role in enhancing photoluminescence in $MoSe_2$. In the following paragraphs we discuss the HBr treatment effect on the doping level, structural defects, and chemical composition and further reveal the mechanism of optical property modulation in $MoSe_2$.

Raman scattering is known to be sensitive to the doping level of 2D materials. We use Raman spectroscopy to investigate the charge-phonon interaction in $MoSe_2$ layers. For a monolayer $MoSe_2$ only one Raman active mode (out-of-plane A_{1g}) appears. Figure 2a shows the typical Raman spectrum for the $MoSe_2$ flakes before and after HBr treatment, where a predominate A_{1g} mode at ~240.4 1/cm is identified for the as-grown $MoSe_2$. The out-of-plane vibrational A_{1g} mode becomes stronger and shifts to a higher frequency at 241.1 1/cm after HBr treatment. Figure 2b shows the statistical measurements for the Raman frequency and Figure 2c shows the Raman intensity mappings for the as-grown and HBr treated $MoSe_2$ monolayers. The A_{1g} mode results from the out-of-plane vibration of Se atoms in opposite directions, which couples more strongly with electrons than the in-plane vibrational mode does. Calculation based on first-principles density functional theory shows that electron doping leads to occupation of the bottom of the conduction band at the K point states resulting in a significant change in the electron-phonon coupling of A_{1g}.[42] It has also been demonstrated experimentally that *n*-doping typically results in the softening and intensity decrease of the A_{1g} phonon while *p*-doping causes the hardening and intensity increase of A_{1g} phonon. [31, 47, 48] Therefore, the A_{1g} phonon renormalization can be used to estimate the doping level change in TMDCs. The intensity increase and frequency upshift in A_{1g} mode suggest that HBr treatment imposes *p*-doping to $MoSe_2$ layers. [49] We provide quantitative analysis of the doping level (details in supporting materials, and Figure S5). The electron carrier density are estimated to be 8.2×10^{11}

cm^{-2} for as-grown and 6.37×10^{10} cm^{-2} for HBr treated $MoSe_2$ respectively, which are within a comparable range with the previous report. [30]

To further reveal the excitonic nature of $MoSe_2$ monolayer and the effect after HBr treatment, we perform temperature dependence PL measurement down to 10 K for the as-grown and HBr-treated $MoSe_2$ layers. Figures 3a compares the PL emission from as-grown and HBr treated $MoSe_2$ at 10K. The neutral exciton of $MoSe_2$ monolayer has been reported to emit at around 1.66 eV [30]. Figure 3a shows that a strong emission at a lower energy (around 1.56 eV) from our as-grown $MoSe_2$ with a full width at half-maximum (FWHM) value of 80.6 meV. The peak at 1.56 eV indicates that the radiative excitons are bound to defects which is in good agreement with the previous report[39] since the defect-related, trapped excitons should lead to an emission energy lower than the band-to-band optical transition energy. After HBr treatment, the defect related PL emission $MoSe_2$ is dramatically suppressed as revealed in Figure 3a. In addition to the broad sub-band-gap emission at around 1.59 eV, we observed two additional peaks at 1.66 and 1.63 eV, assigned as the neutral exciton (X^0) and the trion peak (X^-) respectively.[30] Figure 3b shows the evolution of neutral exciton and trion peaks as a function of temperature from 10 K to 300 K. The trion peak becomes negligible when the temperature is higher than 150 K. Figures 3c and 3d show the temperature dependence of the X^0 and X^- peak position and intensity extracted based on the same fitting method in Figure 3a. Also, a binding energy of 30 meV is extracted, which is in good agreement with previous reports.[30] The temperature dependence of the peak intensity ratio (X^-/ X^0) for $MoSe_2$ monolayers shown in Figure 3d suggests that our $MoSe_2$ sample exhibits a higher trion to exciton ratio. The appearance of X^0 emission suggests that the highly n-doping feature in pristine $MoSe_2$ has been reduced considerably after HBr treatments. [30] The temperature dependence measurement of $MoSe_2$ PL suggests the defects within the as-grown $MoSe_2$ crystals prohibit the intrinsic exciton emission and the dominate PL peak is mostly from trapped exciton states. While for the HBr-treated $MoSe_2$, the trapped exciton state is greatly suppressed, and both exiton and trion peaks are detectable at a low temperature.

Both theoretical [50, 51] and experimental [52, 53] works have demonstrated that the defects such as cation and anion vacancies in TMDCs could induce doping. In order to reveal the as-grown and treated $MoSe_2$ microscopically, $MoSe_2$ monolayers are transferred onto a transmission electron microscope (TEM) grid and visualized under TEM and STEM. The transfer process unavoidably induces the folding of $MoSe_2$ (Top area in Figure 4a). Figure 4b displays the high resolution TEM (HRTEM) image. The inset in Figure 4b corresponds to the Fast Fourier Transform (FFT) of the image Figure 4b, which clearly shows the hexagonal packing of $MoSe_2$ crystals. In addition to the TEM characterization, a more precise lattice structure measurement was carried out using aberration-corrected STEM. We further visualize the flake *via* chemical analysis using atomic-resolution Z-contrast imaging with high-angle annular dark field (HAADF) STEM. As the intensity of STEM images directly related to the atomic number (Z-contrast), individual Se atoms can be easily recognized and differentiated from the three-fold coordinated two Se atoms. Figures 4c and 4d are the STEM images of $MoSe_2$ before and after HBr treatment. By analysing the column-to-column intensity ratio of metal and chalcogen sites in Figures 4c and 4d, the lattice structures have been reconstructed and shown in Figures 4e and 4f. The STEM characterization identifies the presence of large number of single Se vacancies, and we also observe Se point defects in the as-grown $MoSe_2$ layer (as shown in Figure 4c and 4e up right corner). It was found that the individual Se vacancies are stable under TEM. Meanwhile, we note there are no Mo vacancies observed in the examined locations for both of as-grown and HBr treated samples. The presence of Se vacancies contributes to the *n*-doping and PL weakening in $MoSe_2$. We can draw the conclusion that HBr treatment can effectively tailor the localized exciton in $MoSe_2$ defect sites structured by Se vacancies and release the defect bound excitons. Qualitatively, we note that the Se vacancies in HBr treated samples are relatively less than the as-grown $MoSe_2$ monolayers.

To obtain more insights of HBr treatment on the lattice structure of $MoSe_2$, XPS was used to further reveal the chemical composition change of CVD grown $MoSe_2$. As shown in Figure 5a, the binding energies of Mo $3d_{5/2}$ and Mo $3d_{3/2}$ are around 229.4 and 232.53 eV respectively, revealing the +IV oxidation chemical state of Mo. The small shoulder peaks at around 233.3 and 236.43 eV in Figure 5a

can be assigned to Mo $3d_{5/2}$ and $3d_{3/2}$ core levels of the hexa-valent state of Mo[54], originated from not fully selenized MoO_3 precursors used in CVD growth. We note the hexa-valent state becomes barely detectable after HBr treatment, suggesting HBr-treatment can remove these impurities. It is noteworthy, after HBr treatment there is a red shift for the peak positions of $Mo^{(IV)}$ $3d_{5/2}$ and $3d_{3/2}$ from 229.6 eV to 229.4 eV which could suggest a reduction of $Mo^{(IV)}$ oxidation sate or a *p*-doping[55], consistent with the conclusion drawn from Raman measurements. Additionally, the full width at half maximum (FWHM) of $Mo^{(IV)}$ also decreases from 1.53 to 1.06 eV, indicating a more uniform chemical environment for Mo after the HBr treatment. In Figure 5b, the Se $3d_{5/2}$ and $3d_{3/2}$ doublets at (54.8 eV; 55.66 eV) and (55.34 eV; 56.2 eV) can be assigned to terminal Se^{2-} and bridging Se_2^{2-}, respectively[56], and these are the two types of covalent bonds observed in both as-grown and HBr treated $MoSe_2$ layers. The binding energy of $3d_{5/2}$ core levels at 55.9 eV is ascribed to elementary $Se^{(0)}$ impurities originated from Se element or the oxidized $MoSe_2$ (Mo-Se-O) state. The broad peak at around 59.2 eV is attributed to the oxidized Se species such as the SeO_2 impurity [57]. However, these peaks are observable in as-grown but not in HBr-treated $MoSe_2$ layers. It is known that HBr is able to remove the oxygen in SeO_2 thought the formation of $SeBr_4$.[58] We suspect that HBr might be able to remove the oxygen species in oxidized $MoSe_2$, where the Mo-Se-O could be transformed to Mo-Se-Br. This postulation agrees well with the observation of FWHM narrowing for $Mo^{(IV)}$ peak after HBr treatment. The binding energy evolution for Mo, Se and Br is summarized in Table R3 in Supporting Information. Note that the Br^- ions are detected at around 68.6 eV (Br $3d_{5/2}$ doublet) after HBr treatment as shown in Figure 5c, which is confirms the reaction between $MoSe_2$ and HBr. Note that in STEM we could not identify the Br atom since Br has a similar atomic number as Se (35 and 34 respectively). However, we do observe the presence of Br in the XPS and energy-filtered electron energy-loss spectrum (EELS) elementary mapping (shown in Figure S6). This suggests that Br ions adsorb on $MoSe_2$ as counter ions. Since Se and Br are not distinguishable in STEM, we cannot exclude the possibility that Br ions fill in the Se vacancies as illustrated in Figure 5d.

To further strengthen the arguments of structural repairing by HBr, we calculate the elemental ratio of Mo, Se and Br based on their corresponding XPS peak areas. The atomic ratio of anions versus $Mo^{(IV)}$

is shown in Figure 5e. The ratio of as-grown $MoSe_2$ is 1.686 suggesting the presence of the high density of Se vacancies and $Se^{(0)}$ and SeO_2 impurities. Remarkably, after HBr treatment, the anions to Mo atomic ratio increased to 1.97, this increase is majorly contributed from the incorporation of additional Br anions and the increase in Se^{2-}, where the increase is likely from the conversion of the bridging Se_2^{2-} to the Se^{2-}. We also note the SeO_2 becomes undetectable, but with a dramatically increased percentage of Se^{2-}. Revealed by our STEM characterization, the lattice structure defects are mainly the Se vacancies. In brief, all the XPS results suggest that HBr not only *p*-dopes but also removes the impurities $Se^{(0)}$ and SeO_2. Meanwhile, the HBr treatment most likely reduces the Se vacancies by filling Se vacancies using the Se in the bridging form Se_2^{2-} to Se^{2-}. The passivation of Se vacancies with Br ions might also occur at the same time.

CONCLUSIONS

In conclusion, point defects formed by Se vacancies can greatly quench the PL of monolayer $MoSe_2$ due to the trapping of free charge carriers and non-radiative recombination. Low temperature PL study shows that HBr can effectively suppress the trapped exciton states and populate both exciton and trion emission. Other hydrohalic acids such as HCl, and HI also show similar PL enhancement effects. However, HBr is the most effective chemical with a suitable acidity and thus provides better controllability for tailoring the optical properties of $MoSe_2$. The drastic modulation of optical properties by HBr can be attributed to various reasons including removing impurities, *p*-doping to the $MoSe_2$, and reducing the structure of $MoSe_2$. Our method offers the insights for tuning the properties of 2D TMDCs.

METHODS

Growth of $MoSe_2$ layers: We have developed the CVD method to synthesize monolayer $MoSe_2$. The precursor of Mo and Se are MoO_2 powder (Sigma Aldrich, ≧99.5% purity) and Se powder (Sigma Aldrich, ≧99.5% purity), respectively. MoO_2 powder (0.3 g) was placed in a ceramic boat at the center of furnace with a 1 cm ×5 cm sapphire substrate placed at downstream of ceramic boat. Selenium powder was heated by another furnace and carried by Ar/H_2 (Ar/H_2 = 65 sccm/5 sccm, 50 torr). The centre of the furnace was

gradually heated from room temperature to 800 ℃ at the rate of 25 ℃/min. The temperature of the Se powder at the upstream furnace was raised up to 260 ℃ when the growth furnace temperature reached 800 ℃. In order to growing $MoSe_2$ triangle domains, the furnace was held at 800 ℃ for 15 min. After growth, the furnace was naturally cooled down to room temperature.

Chemical treatment of $MoSe_2$ layers: After getting the $MoSe_2$ triangle domains on sapphire substrate, we used hydrobromic acid (Alfa Aesar, 49% liquid) or other hydrohalic acids as a chemical source. The bubble method was performed to spray the HBr droplets onto the sapphire substrate where the $MoSe_2$ domains were prepared. After the evaporation of chemical solvent, the $MoSe_2$ triangle domains were characterized by optical measurements.

Transfer method for pristine and HBr treated $MoSe_2$: The TMDCs layers were transferred onto target substrates or TEM grids by a poly (methyl methacrylate) (PMMA) (950 PMMA A4, Micro Chem) assisted method. First PMMA thin film was spin-coated on top of the sample, and then the PMMA/$MoSe_2$/sapphire was dipped in a 6M HF solution to etch the $MoSe_2$/sapphire interface. PMMA/$MoSe_2$ was lifted from the etching solution and diluted in DI water, and then transferred onto target substrates. The PMMA layer was removed with acetone and isopropanol.

Characterizations: The aberration-corrected JEOL-2100F cold field emission gun electron microscope equipped with a DELTA corrector was used to observe the annular dark field (ADF) images in this work. The ADF images were obtained at an accelerating voltage of 60 kV at room temperature. The probe current we used to detect was about 10~15 pA. The scanning rate of the ADF images was set in the region of 8 to 128 μs/pixel. Photoluminescence spectra and Raman spectra were excited by a green laser with 532 nm wavelength in a Witec alpha 300 confocal Raman microscopic system. The spot size of laser beam is about 0.5 μm and a 0.9 N.A. of 100X objective from Carl Zeiss Microscopy GmbH was used to collected the emitted Raman (1800 lines/mm grating) and PL signal (300 lines/mm grating). A higher grating was used to obtain more details Raman line shapes. The Raman wavelength calibration used the

Si Raman peak which is at 520 cm^{-1} to be a reference. The sample was cooled down to T = 4 K in a low-vibration cryogen-free cryostat for the low-temperature PL measurement. A 0.42 N.A. objective lens was used in the 4K low-temperature measurement for having long working distance. Chemical configurations were determined by X-ray photoelectron spectroscopy (XPS, Phi V5000). XPS measurements were performed with an Al Kα X-ray source on the samples. The energy calibrations were made against the C 1s peak to eliminate the charging of the sample during analysis.

ACKNOWLEDGMENTS: L.-J.L. and Y. Shi acknowledge support from King Abdullah University of Science and Technology (Saudi Arabia). L.-J.L. Acknowledges Ministry of Science and Technology (MOST) and Taiwan Consortium of Emergent Crystalline Materials (TCECM), Academia Sinica (Taiwan), and AOARD-134137 (USA). H.-C.K. acknowledges the support from MOST of Taiwan under grant NSC104-3113-E-009-002-CC2. Y.-C.L. and K.S. acknowledge support from the Japan Science and Technology Agency research acceleration program. W.-H.C. acknowledges the support from TCECM, MOST of Taiwan under grant NSC102-2119-M-009-002-MY3 and the Center for Interdisciplinary Science of Nation Chiao Tung University.

Supporting Information Available: Figures S1-S3 are included. This material is available free of charge *via* the Internet at http://pubs.acs.org.

REFERENCES

1. RadisavljevicB; RadenovicA; BrivioJ; GiacomettiV; KisA. Single-layer MoS_2 Transistors. *Nat. Nanotechnol.* 2011, 6, 147-150.
2. Lee, C.; Yan, H.; Brus, L. E.; Heinz, T. F.; Hone, J.; Ryu, S. Anomalous Lattice Vibrations of Single- and Few-Layer MoS_2. *ACS Nano* 2010, 4, 2695-2700.
3. Zhang, X.; Lai, Z.; Liu, Z.; Tan, C.; Huang, Y.; Li, B.; Zhao, M.; Xie, L.; Huang, W.; Zhang, H. A Facile and Universal Top-Down Method for Preparation of Monodisperse Transition-Metal Dichalcogenide Nanodots. *Angew. Chem., Int. Ed.* 2015, 54, 5425-5428.
4. Zhang, W.; Chiu, M.-H.; Chen, C.-H.; Chen, W.; Li, L.-J.; Wee, A. T. S. Role of Metal Contacts in High-Performance Phototransistors Based on WSe_2 Monolayers. *ACS Nano* 2014, 8, 8653-8661.
5. Pu, J.; Yomogida, Y.; Liu, K.-K.; Li, L.-J.; Iwasa, Y.; Takenobu, T. Highly Flexible MoS_2 Thin-Film Transistors with Ion Gel Dielectrics. *Nano Lett.* 2012, 12, 4013-4017.

6. Zhu, C.; Zeng, Z.; Li, H.; Li, F.; Fan, C.; Zhang, H. Single-Layer MoS_2-Based Nanoprobes for Homogeneous Detection of Biomolecules. *J. Am. Chem. Soc.* 2013, 135, 5998-6001.
7. Loan, P. T. K.; Zhang, W.; Lin, C.-T.; Wei, K.-H.; Li, L.-J.; Chen, C.-H. Graphene/MoS_2 Heterostructures for Ultrasensitive Detection of DNA Hybridisation. *Adv. Mater.* 2014, 26, 4838-4844.
8. Li, H.; Shi, Y.; Chiu, M.-H.; Li, L.-J. Emerging Energy Applications of Two-Dimensional Layered Transition Metal Dichalcogenides. *Nano Energy* 2015, 18, 293-305.
9. Liu, W.; Kang, J.; Sarkar, D.; Khatami, Y.; Jena, D.; Banerjee, K. Role of Metal Contacts in Designing High-Performance Monolayer n-Type WSe_2 Field Effect Transistors. *Nano Lett.* 2013, 13, 1983-1990.
10. Chang, Y.-H.; Nikam, R. D.; Lin, C.-T.; Huang, J.-K.; Tseng, C.-C.; Hsu, C.-L.; Cheng, C.-C.; Su, C.-Y.; Li, L.-J.; Chua, D. H. C. Enhanced Electrocatalytic Activity of MoS_x on TCNQ-Treated Electrode for Hydrogen Evolution Reaction. *ACS Appl. Mater. Interfaces* 2014, 6, 17679-17685.
11. Chang, Y.-H.; Lin, C.-T.; Chen, T.-Y.; Hsu, C.-L.; Lee, Y.-H.; Zhang, W.; Wei, K.-H.; Li, L.-J. Highly Efficient Electrocatalytic Hydrogen Production by MoS_x Grown on Graphene-Protected 3D Ni Foams. *Adv. Mater.* 2013, 25, 756-760.
12. Shi, Y.; Wang, Y.; Wong, J. I.; Tan, A. Y. S.; Hsu, C.-L.; Li, L.-J.; Lu, Y.-C.; Yang, H. Y. Self-assembly of Hierarchical MoS_x/CNT Nanocomposites: Towards High Performance Anode Materials for Lithium Ion Batteries. *Sci. Rep.* 2013, 3, 2169.
13. Stephenson, T.; Li, Z.; Olsen, B.; Mitlin, D. Lithium Ion Battery Applications of Molybdenum Disulfide (MoS_2) Nanocomposites. *Energy Environ. Sci.* 2014, 7, 209-231.
14. Lee, Y.-H.; Zhang, X.-Q.; Zhang, W.; Chang, M.-T.; Lin, C.-T.; Chang, K.-D.; Yu, Y.-C.; Wang, J. T.-W.; Chang, C.-S.; Li, L.-J.; Lin, T.-W. Synthesis of Large-Area MoS_2 Atomic Layers with Chemical Vapor Deposition. *Adv. Mater.* 2012, 24, 2320-2325.
15. Liu, K.-K.; Zhang, W.; Lee, Y.-H.; Lin, Y.-C.; Chang, M.-T.; Su, C.-Y.; Chang, C.-S.; Li, H.; Shi, Y.; Zhang, H.; Lai, C.-S.; Li, L.-J. Growth of Large-Area and Highly Crystalline MoS_2 Thin Layers on Insulating Substrates. *Nano Lett.* 2012, 12, 1538-1544.
16. Shi, J.; Ma, D.; Han, G.-F.; Zhang, Y.; Ji, Q.; Gao, T.; Sun, J.; Song, X.; Li, C.; Zhang, Y.; Lang, X.-Y.; Zhang, Y.; Liu, Z. Controllable Growth and Transfer of Monolayer MoS_2 on Au Foils and Its Potential Application in Hydrogen Evolution Reaction. *ACS Nano* 2014, 8, 10196-10204.
17. Gutiérrez, H. R.; Perea-López, N.; Elías, A. L.; Berkdemir, A.; Wang, B.; Lv, R.; López-Urías, F.; Crespi, V. H.; Terrones, H.; Terrones, M. Extraordinary Room-Temperature Photoluminescence in Triangular WS_2 Monolayers. *Nano Lett.* 2013, 13, 3447-3454.
18. Zhang, Y.; Zhang, Y.; Ji, Q.; Ju, J.; Yuan, H.; Shi, J.; Gao, T.; Ma, D.; Liu, M.; Chen, Y.; Song, X.; Hwang, H. Y.; Cui, Y.; Liu, Z. Controlled Growth of High-Quality Monolayer WS_2 Layers on Sapphire and Imaging Its Grain Boundary. *ACS Nano* 2013, 7, 8963-8971.
19. Gao, Y.; Liu, Z.; Sun, D.-M.; Huang, L.; Ma, L.-P.; Yin, L.-C.; Ma, T.; Zhang, Z.; Ma, X.-L.; Peng, L.-M.; Cheng, H.-M.; Ren, W. Large-area Synthesis of High-quality and Uniform Monolayer WS_2 on Reusable Au Foils. *Nat. Commun.* 2015, 6, 8569.
20. Wang, X.; Gong, Y.; Shi, G.; Chow, W. L.; Keyshar, K.; Ye, G.; Vajtai, R.; Lou, J.; Liu, Z.; Ringe, E.; Tay, B. K.; Ajayan, P. M. Chemical Vapor Deposition Growth of Crystalline Monolayer $MoSe_2$. *ACS Nano* 2014, 8, 5125-5131.
21. Chang, Y.-H.; Zhang, W.; Zhu, Y.; Han, Y.; Pu, J.; Chang, J.-K.; Hsu, W.-T.; Huang, J.-K.; Hsu, C.-L.; Chiu, M.-H.; Takenobu, T.; Li, H.; Wu, C.-I.; Chang, W.-H.; Wee, A. T. S.; Li, L.-J. Monolayer $MoSe_2$ Grown by Chemical Vapor Deposition for Fast Photodetection. *ACS Nano* 2014, 8, 8582-8590.
22. Liu, B.; Fathi, M.; Chen, L.; Abbas, A.; Ma, Y.; Zhou, C. Chemical Vapor Deposition Growth of Monolayer WSe_2 with Tunable Device Characteristics and Growth Mechanism Study. *ACS Nano* 2015, 9, 6119-6127.
23. Fang, H.; Chuang, S.; Chang, T. C.; Takei, K.; Takahashi, T.; Javey, A. High-Performance Single Layered WSe_2 p-FETs with Chemically Doped Contacts. *Nano Lett.* 2012, 12, 3788-3792.

24. Huang, J.-K.; Pu, J.; Hsu, C.-L.; Chiu, M.-H.; Juang, Z.-Y.; Chang, Y.-H.; Chang, W.-H.; Iwasa, Y.; Takenobu, T.; Li, L.-J. Large-Area Synthesis of Highly Crystalline WSe_2 Monolayers and Device Applications. *ACS Nano* 2014, 8, 923-930.
25. Chen, L.; Liu, B.; Ge, M.; Ma, Y.; Abbas, A. N.; Zhou, C. Step-Edge-Guided Nucleation and Growth of Aligned WSe_2 on Sapphire via a Layer-over-Layer Growth Mode. *ACS Nano* 2015, 9, 8368-8375.
26. Wang, Q. H.; Kalantar-Zadeh, K.; Kis, A.; Coleman, J. N.; Strano, M. S. Electronics and Optoelectronics of Two-dimensional Transition Metal Dichalcogenides. *Nat. Nanotechnol.* 2012, 7, 699-712.
27. Jo, S.; Ubrig, N.; Berger, H.; Kuzmenko, A. B.; Morpurgo, A. F. Mono- and Bilayer WS_2 Light-Emitting Transistors. *Nano Lett.* 2014, 14, 2019-2025.
28. Yin, Z.; Li, H.; Li, H.; Jiang, L.; Shi, Y.; Sun, Y.; Lu, G.; Zhang, Q.; Chen, X.; Zhang, H. Single-Layer MoS_2 Phototransistors. *ACS Nano* 2012, 6, 74-80.
29. Zhang, W.; Huang, J.-K.; Chen, C.-H.; Chang, Y.-H.; Cheng, Y.-J.; Li, L.-J. High-Gain Phototransistors Based on a CVD MoS_2 Monolayer. *Adv. Mater.* 2013, 25, 3456-3461.
30. Ross, J. S.; Wu, S.; Yu, H.; Ghimire, N. J.; Jones, A. M.; Aivazian, G.; Yan, J.; Mandrus, D. G.; Xiao, D.; Yao, W.; Xu, X. Electrical Control of Neutral and Charged Excitons in a Monolayer Semiconductor. *Nat. Commun.* 2013, 4, 1474.
31. Peimyoo, N.; Yang, W.; Shang, J.; Shen, X.; Wang, Y.; Yu, T. Chemically Driven Tunable Light Emission of Charged and Neutral Excitons in Monolayer WS_2. *ACS Nano* 2014, 8, 11320-11329.
32. Mouri, S.; Miyauchi, Y.; Matsuda, K. Tunable Photoluminescence of Monolayer MoS_2 via Chemical Doping. *Nano Lett.* 2013, 13, 5944-5948.
33. Nan, H.; Wang, Z.; Wang, W.; Liang, Z.; Lu, Y.; Chen, Q.; He, D.; Tan, P.; Miao, F.; Wang, X.; Wang, J.; Ni, Z. Strong Photoluminescence Enhancement of MoS_2 through Defect Engineering and Oxygen Bonding. *ACS Nano* 2014, 8, 5738-5745.
34. Sigle, D. O.; Mertens, J.; Herrmann, L. O.; Bowman, R. W.; Ithurria, S.; Dubertret, B.; Shi, Y.; Yang, H. Y.; Tserkezis, C.; Aizpurua, J.; Baumberg, J. J. Monitoring Morphological Changes in 2D Monolayer Semiconductors Using Atom-Thick Plasmonic Nanocavities. *ACS Nano* 2015, 9, 825-830.
35. Sanfeng, W.; Sonia, B.; Aaron, M. J.; Jason, S. R.; Nirmal, J. G.; Jiaqiang, Y.; David, G. M.; Wang, Y.; Fariba, H.; Jelena, V.; Arka, M.; Xiaodong, X. Control of Two-dimensional Excitonic Light Emission via Photonic Crystal. *2D Mater.* 2014, 1, 011001.
36. Hui, Y. Y.; Liu, X.; Jie, W.; Chan, N. Y.; Hao, J.; Hsu, Y.-T.; Li, L.-J.; Guo, W.; Lau, S. P. Exceptional Tunability of Band Energy in a Compressively Strained Trilayer MoS_2 Sheet. *ACS Nano* 2013, 7, 7126-7131.
37. Li, M.-Y.; Shi, Y.; Cheng, C.-C.; Lu, L.-S.; Lin, Y.-C.; Tang, H.-L.; Tsai, M.-L.; Chu, C.-W.; Wei, K.-H.; He, J.-H.; Chang, W.-H.; Suenaga, K.; Li, L.-J. Epitaxial Growth of a Monolayer WSe_2-MoS_2 Lateral p-n Junction with an Atomically Sharp Interface. *Science* 2015, 349, 524-528.
38. Chow, P. K.; Jacobs-Gedrim, R. B.; Gao, J.; Lu, T.-M.; Yu, B.; Terrones, H.; Koratkar, N. Defect-Induced Photoluminescence in Monolayer Semiconducting Transition Metal Dichalcogenides. *ACS Nano* 2015, 9, 1520-1527.
39. Tongay, S.; Suh, J.; Ataca, C.; Fan, W.; Luce, A.; Kang, J. S.; Liu, J.; Ko, C.; Raghunathanan, R.; Zhou, J.; Ogletree, F.; Li, J.; Grossman, J. C.; Wu, J. Defects Activated Photoluminescence in Two-dimensional Semiconductors: Interplay between Bound, Charged, and Free Excitons. *Sci. Rep.* 2013, 3, 2657.
40. Peimyoo, N.; Shang, J.; Cong, C.; Shen, X.; Wu, X.; Yeow, E. K. L.; Yu, T. Nonblinking, Intense Two-Dimensional Light Emitter: Monolayer WS_2 Triangles. *ACS Nano* 2013, 7, 10985-10994.
41. Lukowski, M. A.; Daniel, A. S.; Meng, F.; Forticaux, A.; Li, L.; Jin, S. Enhanced Hydrogen Evolution Catalysis from Chemically Exfoliated Metallic MoS_2 Nanosheets. *J. Am. Chem. Soc.* 2013, 135, 10274-10277.
42. Kibsgaard, J.; Chen, Z.; Reinecke, B. N.; Jaramillo, T. F. Engineering the Surface Structure of MoS_2 to Preferentially Expose Active Edge Sites for Electrocatalysis. *Nat. Mater.* 2012, 11, 963-969.

43. Amani, M.; Lien, D.-H.; Kiriya, D.; Xiao, J.; Azcatl, A.; Noh, J.; Madhvapathy, S. R.; Addou, R.; KC, S.; Dubey, M.; Cho, K.; Wallace, R. M.; Lee, S.-C.; He, J.-H.; Ager, J. W.; Zhang, X.; Yablonovitch, E.; Javey, A. Near-unity Photoluminescence Quantum Yield in MoS_2. *Science* 2015, 350, 1065-1068.
44. Shi, Y.; Li, H.; Li, L.-J. Recent Advances in Controlled Synthesis of Two-dimensional Transition Metal Dichalcogenides via Vapour Deposition Techniques. *Chem. Soc. Rev.* 2015, 44, 2744-2756.
45. McDonnell, S.; Addou, R.; Buie, C.; Wallace, R. M.; Hinkle, C. L. Defect-Dominated Doping and Contact Resistance in MoS_2. *ACS Nano* 2014, 8, 2880-2888.
46. Tongay, S.; Zhou, J.; Ataca, C.; Liu, J.; Kang, J. S.; Matthews, T. S.; You, L.; Li, J.; Grossman, J. C.; Wu, J. Broad-Range Modulation of Light Emission in Two-Dimensional Semiconductors by Molecular Physisorption Gating. *Nano Lett.* 2013, 13, 2831-2836.
47. Shi, Y.; Huang, J.-K.; Jin, L.; Hsu, Y.-T.; Yu, S. F.; Li, L.-J.; Yang, H. Y. Selective Decoration of Au Nanoparticles on Monolayer MoS_2 Single Crystals. *Sci. Rep.* 2013, 3, 1839.
48. Chakraborty, B.; Bera, A.; Muthu, D. V. S.; Bhowmick, S.; Waghmare, U. V.; Sood, A. K. Symmetry-dependent Phonon Renormalization in Monolayer MoS_2 Transistor. *Phys. Rev. B* 2012, 85, 161403.
49. Tonndorf, P.; Schmidt, R.; Böttger, P.; Zhang, X.; Börner, J.; Liebig, A.; Albrecht, M.; Kloc, C.; Gordan, O.; Zahn, D. R. T.; Michaelis de Vasconcellos, S.; Bratschitsch, R. Photoluminescence Emission and Raman Response of Monolayer MoS_2, $MoSe_2$, and WSe_2. *Opt. Express* 2013, 21, 4908-4916.
50. Ma, Y.; Dai, Y.; Guo, M.; Niu, C.; Lu, J.; Huang, B. Electronic and Magnetic Properties of Perfect, Vacancy-doped, and Nonmetal Adsorbed $MoSe_2$, $MoTe_2$ and WS_2 Monolayers. *Phys. Chem. Chem. Phys.* 2011, 13, 15546-15553.
51. Feng, L.-p.; Su, J.; Chen, S.; Liu, Z.-t. First-principles Investigations on Vacancy Formation and Electronic Structures of Monolayer MoS_2. *Mater. Chem. Phys.* 2014, 148, 5-9.
52. Lehtinen, O.; Komsa, H.-P.; Pulkin, A.; Whitwick, M. B.; Chen, M.-W.; Lehnert, T.; Mohn, M. J.; Yazyev, O. V.; Kis, A.; Kaiser, U.; Krasheninnikov, A. V. Atomic Scale Microstructure and Properties of Se-Deficient Two-Dimensional $MoSe_2$. *ACS Nano* 2015, 9, 3274-3283.
53. Kim, B. H.; Park, M.; Lee, M.; Baek, S. J.; Jeong, H. Y.; Choi, M.; Chang, S. J.; Hong, W. G.; Kim, T. K.; Moon, H. R.; Park, Y. W.; Park, N.; Jun, Y. Effect of Sulphur Vacancy on Geometric and Electronic Structure of MoS_2 Induced by Molecular Hydrogen Treatment at Room Temperature. *RSC Adv.* 2013, 3, 18424-18429.
54. Abdallah, W. e.; Nelson, A. E. Characterization of $MoSe_2$(0001) and ion-sputtered $MoSe_2$ by XPS. *J. Mater. Sci.* 2005, 40, 2679-2681.
55. Chiu, M.-H.; Zhang, C.; Shiu, H.-W.; Chuu, C.-P.; Chen, C.-H.; Chang, C.-Y. S.; Chen, C.-H.; Chou, M.-Y.; Shih, C.-K.; Li, L.-J. Determination of Band Alignment in the Single-layer MoS_2/WSe_2 Heterojunction. *Nat. Commun.* 2015, 6.
56. Canava, B.; Vigneron, J.; Etcheberry, A.; Guillemoles, J. F.; Lincot, D. High Resolution XPS Studies of Se Chemistry of a Cu(In, Ga)Se_2 Surface. *Appl. Surf. Sci.* 2002, 202, 8-14.
57. Bachvarova-Nedelcheva, A.; Iordanova, R.; Kostov, K. L.; Yordanov, S.; Ganev, V. Structure and Properties of a Non-traditional Glass Containing TeO_2, SeO_2 and MoO_3. *Opt. Mater.* 2012, 34, 1781-1787.
58. Mews, R. To Give the Se-Halogen Bond. In *Inorganic Reactions and Methods: The Formation of Bonds to Halogens (Part 1)*, Zuckerman, J. J., Hagen, A. P., Eds.; John Wiley & Sons, Inc.: Hoboken, 1989; 3, pp 56-58.